ACS OMEGA

http://pubs.acs.org/journal/acsodf

Article

The Phosphofurin Acidic Cluster Sorting Protein 2 (PACS-2) E209K Mutation Responsible for PACS-2 Syndrome Increases Susceptibility to Apoptosis

Rong Xuan Zang, Mitchell J. Mumby, and Jimmy D. Dikeakos*

Cite This: *ACS Omega* 2022, 7, 34378−34388

Read Online

ACCESS | Metrics & More | Article Recommendations | Supporting Information

ABSTRACT: Phosphofurin acidic cluster sorting protein 2 (PACS-2) is a multifunctional cytosolic membrane trafficking protein with distinct roles in maintaining cellular homeostasis. Recent clinical reports have described 28 individuals possessing a *de novo* PACS-2 E209K mutation that present with epileptic seizures and cerebellar dysgenesis. As the PACS-2 E209K missense mutation has become a marker for neurodevelopmental disorders, we sought to characterize its biochemical properties. Accordingly, we observed that the PACS-2 E209K protein exhibited a slower turnover rate relative to PACS-2 wild type (WT) upon cycloheximide treatment in 293T cells. The longer half-life of PACS-2 E209K suggests a disruption in its proteostasis, with the potential for altered protein−protein interactions. Indeed, a regulatory protein in neurodevelopment known as 14-3-3ε was identified as having an increased association with PACS-2 E209K. Subsequently, when comparing the effect of PACS-2 WT and E209K expression on the staurosporine-induced apoptosis response, we found that PACS-2 E209K increased susceptibility to staurosporine-induced apoptosis in HCT 116 cells. Overall, our findings suggest PACS-2 E209K alters PACS-2 proteostasis and favors complex formation with 14-3-3ε, leading to increased cell death in the presence of environmental stressors.

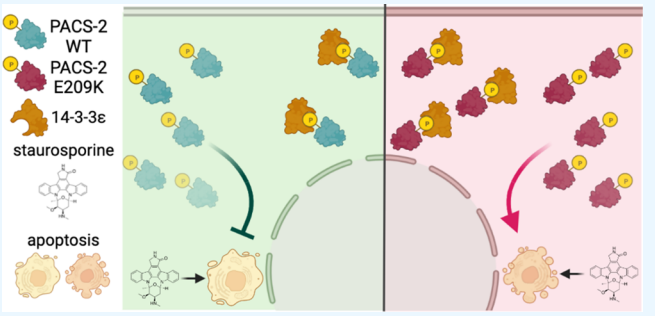

INTRODUCTION

Phosphofurin acidic cluster sorting protein 2 (PACS-2) mediates the trafficking of protein cargo between the endoplasmic reticulum (ER), Golgi, mitochondria, lysosomes, and plasma membrane.[1−5] The PACS-2 N-terminal furin binding region (FBR) coordinates the interactions between the cargo in tandem with adaptor proteins to facilitate protein trafficking to different subcellular localizations (Figure 1A).[6] Notably, the PACS-2 FBR recognizes acidic amino acid residues on the cargo and subsequently associates with the coat protein complex I (COPI) coatomer to mediate the Golgi−ER retrograde trafficking of various proteins, including profurin, calnexin, and polycystin 2.[4,5,7]

In addition to the FBR, PACS-2 contains two domains known as the middle region (MR) and the C-terminal region (CTR) (Figure 1A).[8] Unlike the FBR, the MR does not actively partake in trafficking but instead contains multiple predicted phosphorylation sites for protein−protein interactions.[8,9] Moreover, it has been postulated that the MR autoregulates PACS-2 function between cellular repair, growth, and death, thereby influencing biochemical pathways beyond protein trafficking.[8] Indeed, a nuclear localization signal (NLS, $_{232}$PKKQRRSIV$_{240}$) and a 14-3-3 binding site ($_{434}$RSTpSLKERQ$_{442}$) have been mapped to the PACS-2 MR. The NLS enables PACS-2 recognition by importins, and subsequent PACS-2 nuclear translocation inhibits sirtuin 1 (SIRT1) to promote DNA repair in response to DNA damage.[10,11] Furthermore, the PACS-2 MR also interacts with the 14-3-3 protein family upon phosphorylation by protein kinase B (Akt) at PACS-2 S$_{437}$.[12] Phosphorylated PACS-2 in complex with 14-3-3 promotes lipid biogenesis and inhibits tumor necrosis factor-related apoptosis-inducing ligand (TRAIL)-mediated apoptosis.[12,13]

It was recently reported that at least 28 unrelated individuals displayed a heterozygous c. 625G>A (p. E209K, henceforth referred to as E209K) *de novo* missense mutation within the PACS-2 MR (Figure 1A).[14−23] In addition, individuals harboring PACS-2 E209K polymorphism clinically present with postnatal epileptic seizures and various forms of cranial malformations.[14] These symptoms associated with the E209K mutation were formally denoted as developmental and epileptic encephalopathy 66 (DEE66) by the NIH MedGen database.[24] Collectively, DEE66 corresponds to central

Received: June 27, 2022
Accepted: September 6, 2022
Published: September 15, 2022

https://doi.org/10.1021/acsomega.2c04014
ACS Omega 2022, 7, 34378−34388

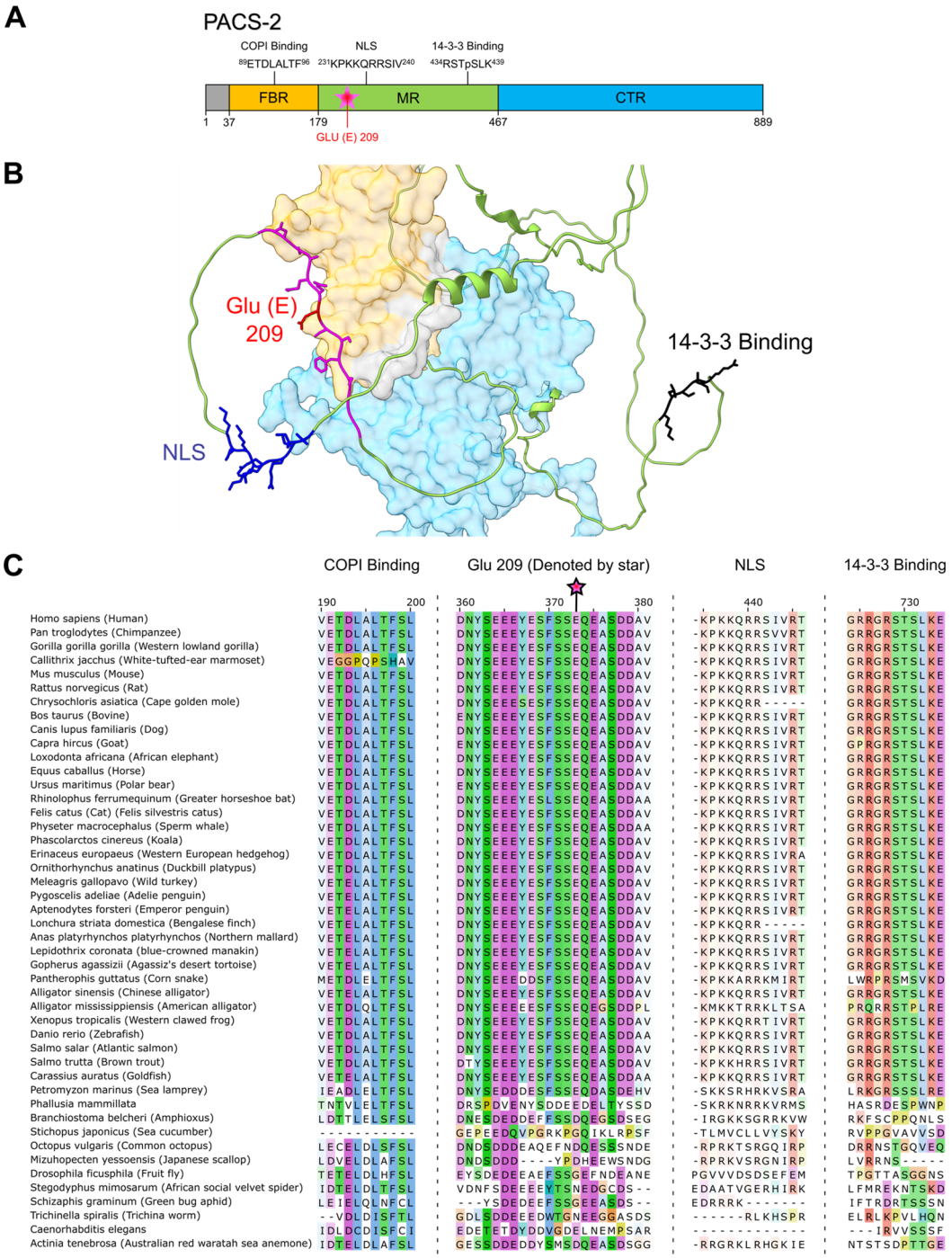

Figure 1. PACS-2 E209 positioned in the MR is well-conserved in chordates. (A) Ribbon diagram depicting the three domains of human PACS-2 (FBR, furin-binding region; MR, middle region; and CTR, C-terminal region). Characterized PACS-2 motifs are marked above the ribbon (NLS, nuclear localization signal). The star indicates the location of E209 implicated in developmental epileptic encephalopathy. (B) Human PACS-2 MR *ab initio* structure as predicted by AlphaFold2. The NLS is colored blue, the amino acids flanking E209 (red) are colored magenta, and the 14-3-3 binding or Akt phosphorylation site is colored black. The FBR, MR, and CTR are transparently colored yellow, green, and blue, respectively. (C) Schematic of human PACS-2 motifs aligned across multiple species. Numerical values on the alignment represent the aligned residue position. The star represents the residue location of the human PACS-2 E209 residue. Hydrophobic residues are highlighted in blue, aromatic residues are highlighted in cyan, polar residues are highlighted in green, basic residues are highlighted in red, acidic residues are highlighted in magenta, cysteines are highlighted in pink, glycine residues are highlighted in orange, proline residues are highlighted in yellow, nonconserved residues are highlighted in white, and dashes represent alignment gaps. The relative color transparency corresponds to residue conservation.

nervous system phenotypes derived from disrupted cellular homeostasis.[14] However, the disease's molecular pathogenesis and the biochemical significance of the PACS-2 E209K mutation remain elusive.

RESULTS AND DISCUSSION

We first retrieved a PACS-2 *ab initio* structure from AlphaFold2 to visualize the secondary and tertiary structures of the PACS-2 domains (Figure S1A).[25,26] Interestingly, the

https://doi.org/10.1021/acsomega.2c04014
ACS Omega 2022, 7, 34378−34388

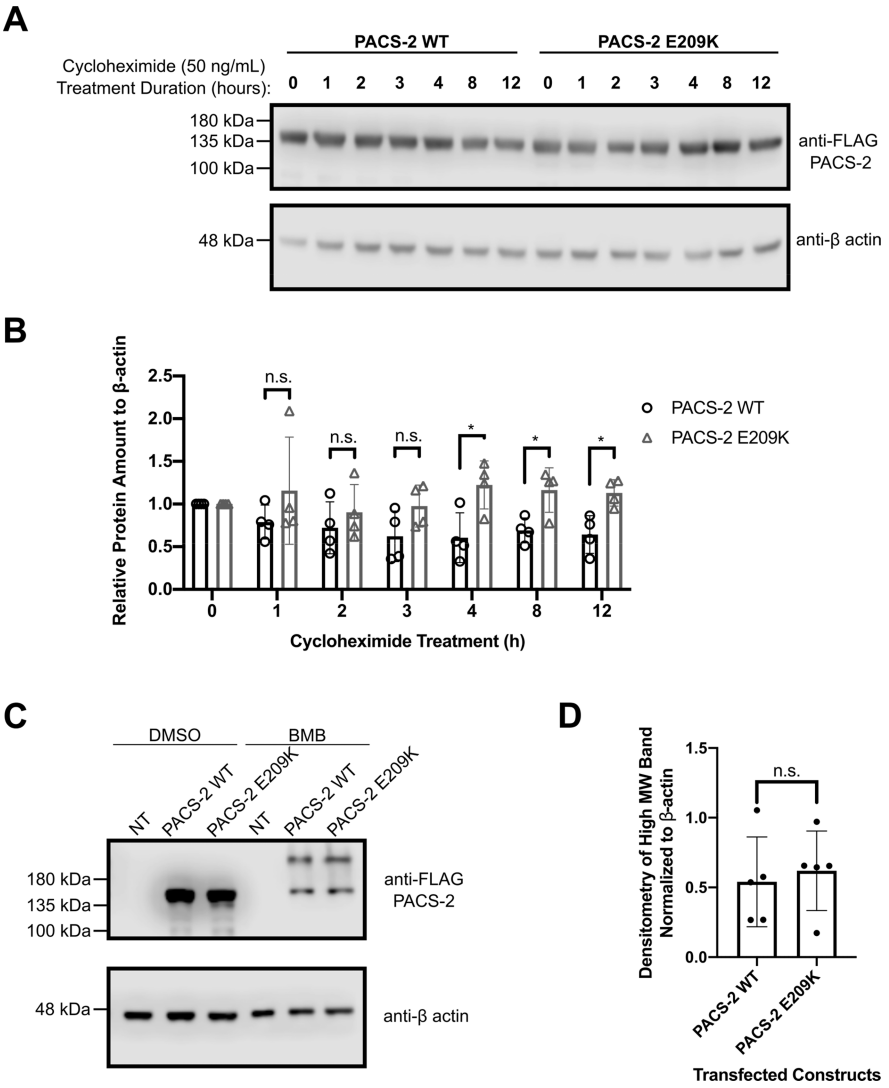

Figure 2. PACS-2 E209K exhibits a longer half-life post-cycloheximide treatment. (A) 293T cells expressing PACS-2 WT or PACS-2 E209K were pulsed with cycloheximide, and whole-cell lysates were harvested at several time intervals post-treatment. A representative Western blot of cell lysates from three independent repeats is shown. Values on the side of the Western blot indicate the approximate molecular weight of the protein ladder in kilodaltons (kDa). (B) Densitometry analysis performed on Western blots. The PACS-2 WT or E209K protein amount was normalized to the β-actin amount before being calculated as a ratio of relative amount to the 0 h time point before the cycloheximide treatment. Unpaired Student's *t*-tests were applied to each time point with a 95% confidence interval ($\alpha = 0.05$; ns, not significant; $^{*}p < 0.05$; $^{**}p < 0.01$; $N = 4$); bars on the scatter plot show the mean with the standard deviation (s.d.). (C) 293T cells expressing PACS-2 WT or PACS-2 E209K were cross-linked with 1,4-bismaleimidobutane (BMB), and whole-cell lysates were harvested. A representative Western blot of cell lysates from five independent repeats is shown. Values on the side of the Western blot indicate the approximate molecular weight of the protein ladder in kDa. NT, non-transfected. (D) Densitometry analysis was performed on Western blots. The bands of oligomeric PACS-2 WT or E209K in BMB-treated samples at ~220 kDa were normalized to β-actin. MW, molecular weight. Unpaired Student's *t*-test with a 95% confidence interval ($\alpha = 0.05$; ns, not significant; $N = 5$); bars on the scatter plot show the mean with the standard deviation (s.d.).

model predicts that the PACS-2 MR is an intrinsically disordered region juxtaposed to the more ordered globular structure of the FBR and the CTR (Figure S1B). The residues flanking E209 ($_{196}$DNYSEEEYESFSS**E**$_{209}$QEASDD$_{215}$) exist within a flexible region and may easily participate in protein complex formation or modulate existing protein−protein interactions (Figure 1B).[27] As such, we performed a sequence alignment based on various PACS-2 paralog and ortholog sequences. We determined that E209 was well conserved from vertebrates to marine tunicates such as *Phallusia mammillata* (Figure 1C). Like the PACS-2 NLS and the 14-3-3 binding site, the early emergence of E209 and its conserved nature in vertebrates suggest that this residue has a significant role in PACS-2 cellular functions.

Interestingly, the paralogous PACS-1 protein has also been implicated in the neurodevelopmental disorder known as Schuurs−Hoeijmakers syndrome.[28,29] However, the corresponding PACS-1 R203W mutation is located within the structured FBR region.[28,29] As PACS-2 E209 is located within an intrinsically disordered region of the MR, the charge reversal conferred by the glutamic acid-to-lysine substitution (E209K) represents a net-positive charge increase within the proximal peptide chain, which may modify the biochemical characteristics of the PACS-2 MR. Similar mutations within the intrinsically disordered region of amyloid-β, τ-protein, and

https://doi.org/10.1021/acsomega.2c04014
ACS Omega 2022, 7, 34378−34388

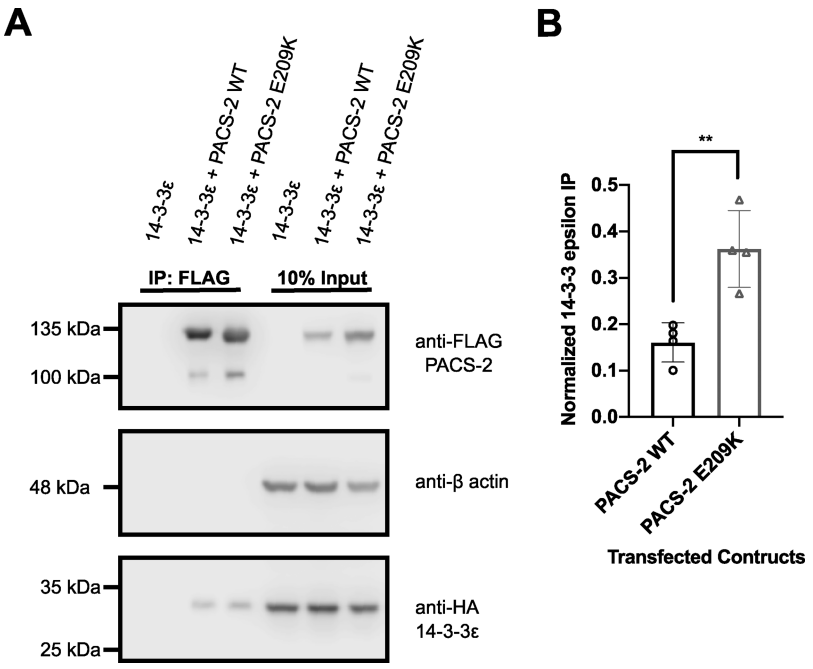

Figure 3. PACS-2 E209K has an enhanced association with 14-3-3ε. (A) 293T cells were transfected with 14-3-3ε alone or cotransfected with 14-3-3ε and the indicated PACS-2 construct. Cell lysates were incubated with anti-FLAG resin for immunoprecipitation (IP) and subjected to Western blot. Numbers on the side of the Western blot indicate the approximate molecular weight of the protein ladder in kDa. (B) Western blot densitometry analysis was based on the ratio of 14-3-3ε IP and the sum of the PACS-2 IP and 14-3-3ε input. Unpaired Student's *t*-test with a 95% confidence interval (α = 0.05; $^{**}p < 0.01$; N = 3); bars on the scatter plot show the mean with the standard deviation (s.d.).

α-synuclein are associated with aberrant expression patterns and interactome profiles that lead to neurodegeneration.[30,31] Thus, we sought to establish the biochemical properties of PACS-2 E209K *in cellulo*. We first evaluated the half-life of the PACS-2 E209K mutant relative to PACS-2 wild type (WT) using a cycloheximide (CHX)-chase assay. CHX blocks ribosomal protein translation, thereby allowing the quantification of the protein half-life. Upon ribosomal inhibition by CHX, the relative protein amount of PACS-2 WT decreased compared to PACS-2 E209K after 4 h of the CHX treatment (PACS-2 amount at 4 h normalized to 0 h: WT = 0.606 versus E209K = 1.223, p = 0.0226) (Figures 2A and B); however, the steady-state levels were equivalent (Figure S2). A prior *in vivo* analysis revealed that PACS-2 cellular activity in the mouse cerebellum is tightly regulated and becomes disrupted in models of Alzheimer's disease. Specifically, PACS-2 protein levels were elevated at two months of age and then drastically declined at six months of age in wild-type mice but not in Alzheimer's disease mice models.[32] The abnormal levels of PACS-2 associated with Alzheimer's disease combined with the dysregulated turnover rate of PACS-2 E209K in DEE66 patients indicate how aberrant PACS-2 proteostasis converges on various neurological defects and symptoms.

A potential sign of disrupted proteostasis is abnormal protein oligomerization, which also increases the protein half-life by reducing the exposure of intrinsically disordered regions on proteins targeted for proteasomal recognition.[33] This phenomenon has been observed for the aforementioned amyloid-β and α-synuclein proteins in the context of neurodegenerative diseases.[34−37] To evaluate the presence of oligomeric PACS-2 complexes, we treated 293T cells expressing PACS-2 WT or E209K with 1,4-bismaleimidobutane (BMB), a homobifunctional sulfhydryl cross-linker. The BMB treatment rendered higher molecular weight (>200 kDa) oligomers for both PACS-2 WT and E209K, while only monomeric (~125 kDa) PACS-2 was observed in the DMSO-treated negative controls (Figures 2C and D). These results demonstrate that both PACS-2 WT and E209K can oligomerize *in cellulo*.

Even though the extent of oligomerization did not differ between PACS-2 WT and E209K, the increased half-life of PACS-2 E209K could be due to decreased ubiquitinoylation, as it was previously reported that PACS-2 could be ubiquitinated.[38] Furthermore, it remains possible that oligomeric complexes may vary in composition. Indeed, mutations in α-synuclein oligomers result in abnormal interactions with RNA binding proteins and mitochondrial proteins, ultimately compromising the molecular machinery and leading to neurodegeneration.[39,40] Thus, the cellular functions of PACS-2 E209K in complex with different proteins could potentially be disrupted, analogous to α-synuclein mutants. To this end, PACS-2 E209K was already shown to favorably interact with histone modulators such as SIRT1 and HDAC1 along with the ion channel protein TRPV1.[14]

Interestingly, PACS-2 also interacts with 14-3-3 proteins as part of the Akt signaling pathway to promote lipid biogenesis by enhancing the association of the ER and mitochondria.[12,13,41] The 14-3-3 protein family consists of dimeric scaffold proteins that bind essential signaling proteins to alter their subcellular localization or enzymatic properties.[42] Furthermore, these proteins are critical for neurodevelopment, as the double knockout of 14-3-3ε and 14-3-3ζ *in vivo* results in neuronal precursor cell migration defects and seizures.[43] Therefore, the potential for PACS-2 to interact with 14-3-3ε to modulate neurodevelopment led us to assess a potential altered association between the 14-3-3ε isoform and both PACS-2 E209K and PACS-2 WT by expressing these proteins in 293T cells. Following coimmunoprecipitation, we found that PACS-

https://doi.org/10.1021/acsomega.2c04014
ACS Omega 2022, 7, 34378−34388

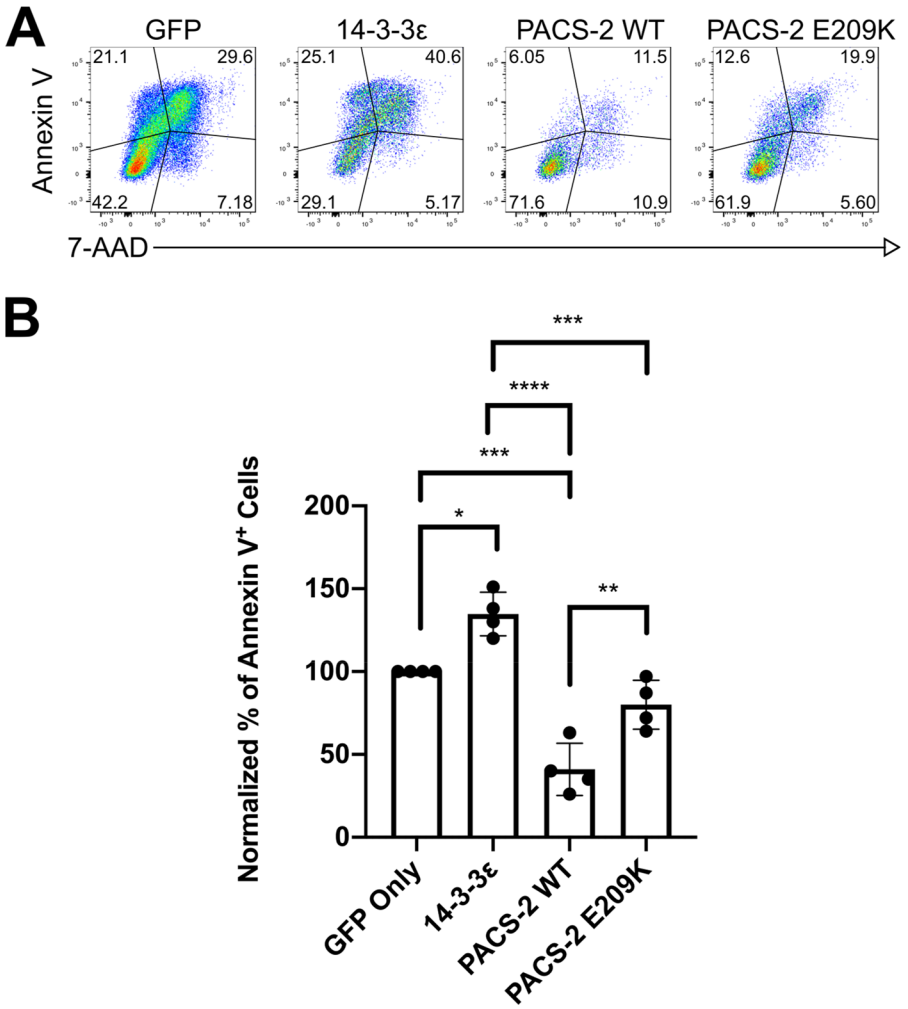

Figure 4. PACS-2 E209K leads to increased susceptibility to apoptosis. (A) HCT116 cells were transfected with GFP, 14-3-3ε-IRES-GFP, PACS2(WT)-IRES-GFP, or PACS2(E209K)-IRES-eGFP, followed by 6 h of 1 μM staurosporine treatment. Treated cells were stained with Pacific Blue Annexin V and 7-AAD for flow cytometry analysis. Representative flow cytometry plots of four independent repeats are shown. Numbers in the corner of the plots represent the percent (%) cell population within each quadrant. (B) Quantification of the healthy cell fraction (Annexin$^-$ and 7-AAD$^-$) and the apoptotic cell fraction (Annexin$^+$) from the overall population. Fractions were normalized to IRES-GFP, which served as a mock control. Statistical comparisons of the fractions were performed separately for the healthy and apoptotic cells. Two-way ANOVA followed by Holm−Šídák multiple-comparison test with a 95% confidence interval (α = 0.05; ns, not significant; *p < 0.05; **p < 0.01; ***p < 0.001; ****p < 0.0001; N = 4); bars on the scatter plot show the mean with the standard deviation (s.d.).

2 E209K demonstrated increased association with 14-3-3ε compared to PACS-2 WT (14-3-3ε association with PACS-2 WT of 0.362 versus that with PACS-2 E209K of 0.161, p = 0.0049) (Figures 3A and B). This increased coimmunoprecipitation was not due to differences in the PACS-2 WT or E209K protein levels (Figure S2). Thus, our observations further illustrate distinct profiles of PACS-2 WT versus E209K oligomeric complexes by demonstrating increased interactions using *bona fide* protein partners in the presence of the E209K mutation.

Functionally, the PACS-2:14-3-3ε interaction prevents PACS-2 from transporting the pro-apoptotic protein BH3 interacting-domain death agonist (Bid) as part of the TRAIL-induced apoptosis pathway.[12] Importantly, apoptosis and other forms of programmed cell death are carefully regulated during neonatal neurodevelopment to facilitate neuroepithelial morphogenesis and synapse formation.[44] Thus, we tested whether PACS-2 E209K dysregulated apoptosis. Accordingly, we inserted an internal ribosomal entry site (IRES) between PACS-2/14-3-3ε and green fluorescent protein (GFP) (Figure S3). Importantly, these constructs showed similar expression levels for PACS-2 WT and E209K while simultaneously expressing GFP for the identification of transfected populations (Figure S4). As 293T cells express the simian vacuolating virus 40 large T antigen, which is known to directly inhibit the initiation of apoptosis, we used HCT116 cells that had previously been used to study PACS-2 and apoptosis.[3,45] HCT116 cells were transfected with pIRES plasmids that encoded 14-3-3ε, PACS-2 WT, or PACS-2 E209K with GFP after the IRES (Figure S3) and treated with the pan-kinase inhibitor staurosporine to induce apoptosis. Our flow cytometry analysis gated cell populations based on GFP$^+$ and Annexin V$^+$ for transfection and apoptosis, respectively (Figure S5). Surprisingly, we noticed a resistance to staurosporine-induced apoptosis for the PACS-2 WT transfected versus the GFP-transfected control population (the PACS-2 WT percent of apoptotic cells normalized to GFP was 41.00, p = 0.0001) (Figures 4A and B). Moreover, the population transfected with PACS-2 E209K had an increased fraction of apoptotic cells compared to those transfected with PACS-2 WT (the percent

https://doi.org/10.1021/acsomega.2c04014
ACS Omega 2022, 7, 34378−34388

of apoptotic cells normalized to GFP for PACS-2 WT was 41.00 and that for E209K was 80.00, $p = 0.0067$) (Figures 4A and B). Interestingly, cells transfected with 14-3-3ε also displayed the highest percentage of apoptotic cells compared to the GFP-transfected cells (the 14-3-3ε percent of apoptotic cells normalized to GFP was 134.8, $p = 0.0111$) (Figures 4A and B). To ensure that expression levels of PACS-2 WT and E209K were comparable within DMSO or staurosporine-treated HCT116 cells using the pIRES-GFP bicistronic constructs, we quantified the mean fluorescence intensity (MFI) of GFP within GFP^+ cells, where the GFP fluorescence was proportional to the expression of the first expressed protein within the bicistronic cassette (i.e., 14-3-3ε, PACS-2 WT, or PACS-2 E209K). We found that, regardless of the DMSO or staurosporine treatment, HCT116 cells expressing PACS-2 WT or PACS-2 E209K did not significantly differ in their level of GFP expression, thereby suggesting the comparable expression of PACS-2 WT and E209K within transfected cells (Figure S6). Interestingly, we found an expected increase in GFP expression for the monocistronic GFP-only control because all the GFP belonged to the second gene under the bicistronic IRES system. Here, we rationalize that the monocistronic GFP only can serve as a negative control because the approximately twofold increase in monocistronic GFP expression accounts for the total amount of protein expression from the two genes in bicistronic constructs and should not affect apoptosis. Collectively, our results suggest that the overexpression of 14-3-3ε or PACS-2 E209K correlates with disrupted signaling, resulting in an increased susceptibility to apoptosis.

Overall, it was unexpected that 14-3-3ε overexpression would increase apoptosis during the staurosporine treatment. This observation contrasted with previous reports that 14-3-3ε is upregulated in various carcinomas to promote survival and counteract cell death.[46−50] Indeed, 14-3-3ε primarily acts as an antiapoptotic protein by sequestering the mitochondrial permeabilizing protein B-cell lymphoma 2-associated agonist of cell death.[46,51] Additionally, 14-3-3ε negatively regulates PACS-2 during TRAIL-induced apoptosis, where it prevents Bid from being trafficked to the mitochondria.[12,52] However, the relationship between staurosporine-induced apoptosis and 14-3-3ε expression levels or a 14-3-3ε:PACS-2 complex has not been examined before, nor has the localization of PACS-2 E209K. The pro-apoptotic effects we observed may be a direct consequence of using different reagents to induce apoptosis. Staurosporine acts as a competitive inhibitor for ATP and functions nonselectively on multiple kinases.[53] Therefore, this inhibition of kinase activity could decrease the number of phosphorylated substrates that canonically bind 14-3-3ε. Furthermore, the cellular environment under the staurosporine treatment could restrict the association of 14-3-3ε with nonphosphorylated substrates, most of which are poorly characterized.[54−56] Thus, our results support the possibility that 14-3-3ε binds to nonphosphorylated proteins during prolonged staurosporine exposure to drive apoptosis as an alternative stress signaling mechanism.

Unlike 14-3-3ε, PACS-2 possesses multiple modes of action on apoptotic pathways, either a positive effect via TRAIL-induced apoptosis,[2,12,38] or a negative effect via the regulation of cell growth, DNA damage, and ER stress.[1,10,57,58] As staurosporine-induced apoptosis is correlated with the upregulation of ER-stress proteins, it was not unexpected that PACS-2 WT overexpression, which directly increases autocrine epidermal growth receptor signaling, decreased apoptosis levels.[1,59] However, the presence of PACS-2 E209K sensitized HCT116 cells to staurosporine-induced apoptosis. As PACS-2 E209K has an enhanced interaction with 14-3-3ε, it remains plausible that the abundance of this protein complex alters the regulatory mode of PACS-2 to subsequently promote apoptosis. The PACS-2:14-3-3 complex may recruit additional 14-3-3 client proteins or alter the pool of PACS-2 substrates to promote apoptosis signaling under extreme stress.

Under the context of neuronal cell signaling, 14-3-3ε binds to the nonphosphorylated Bid apoptotic protein upon seizure-induced neuronal death.[56] Coincidentally, PACS-2 and 14-3-3ε colocalize with Bid at the mitochondria under TRAIL-and staurosporine-associated or seizure-induced cellular stress, respectively.[3,56] Therefore, the enhanced association of PACS-2 E209K with 14-3-3ε may mediate pro-apoptotic signals, particularly during periods of neuronal development.[44] Overall, the increased levels of apoptosis agree with DEE66 patient phenotypes involving epilepsy and cerebellar dysgenesis, as apoptosis can affect neuronal electrical signaling and the developing morphology of the cerebellum.[60−62]

The advent of whole-exome sequencing has resulted in the description of rare *de novo* mutations that are associated with diseased phenotypes or developmental syndromes.[63,64] This advancement has expanded our knowledge of protein networks by going beyond well-established signal transduction proteins and investigating poorly characterized proteins, such as the PACS-2 E209K variant that led to DEE66 in 28 individuals identified thus far.[14−23] We determined that the E209K mutation prolongs the half-life of PACS-2 , leading to an enhanced interaction with 14-3-3ε and an increased susceptibility to apoptosis. These results further our understanding of PACS-2 and implicate various PACS-2:14-3-3 signaling pathways as critical molecular determinants of PACS-2 E209K mutation-related encephalopathies.

MATERIALS AND METHODS

Database Acquisition of the PACS-2 Protein Sequence. PACS-2 sequences from various species were obtained from UniProt; the accession numbers defined in Table S1. Sequences were aligned with Clustal X using the default parameters except for the gap-opening penalty, which was set to 50.[65] Aligned sequences were visualized with Jalview, and the residue identity was colored using the Clustal X color scheme.[65,66]

Cell Culture. Human HEK 293T (ATCC, Manassas, VA) and HCT116 (a generous gift from Dr. Fred Dick at the University of Western Ontario) cell lines were cultured in Dulbecco's modified Eagle's medium (HyClone, Logan, UT) supplemented with 10% fetal bovine serum (Wisent, Quebec, Canada) and 1% penicillin-streptomycin (HyClone). All cell lines were grown at 37 °C in the presence of 5% CO_2 and subcultured following the supplier's recommendations. Cultured cells were routinely screened with the MycoAlert Mycoplasma Detection Kit (Lonza, Basel, Switzerland).

Plasmid and Chemicals. A full-length pcDNA3.1-PACS2-FLAG (PACS-2 WT) plasmid was obtained from Dr. Gary Thomas (University of Pittsburgh School of Medicine, Pittsburgh, PA). The pcDNA3.1-PACS2(E209K)-FLAG (PACS-2 E209K) mutant was generated by overlapping PCR mutagenesis using pcDNA3.1-PACS2(WT)-FLAG as a template.[67] Dual-expressing pIRES-14-3-3ε-HA-IRES-14-3-3ζ-myc was a gift from Dr. Huda Y Zoghbi,[68] and pN1-

https://doi.org/10.1021/acsomega.2c04014
ACS Omega 2022, 7, 34378−34388

eGFP was used as previously described.[69,70] Modified dual-expressing pIRES-14-3-3ε-HA-IRES-eGFP was generated from the pIRES-14-3-3ε-HA-IRES-14-3-3ζ-myc backbone by restriction site cloning to swap the 14-3-3ζ-myc gene with eGFP from pN1-eGFP. The PACS-2 dual-expressing pIRES-PACS2-(WT)-IRES-eGFP and pIRES-PACS2(E209K)-FLAG-IRES-eGFP were generated from pIRES-14-3-3ε-HA-IRES-eGFP by restriction site cloning to swap out 14-3-3ε-HA with PACS2(WT) or PACS2(E209K) from the pcDNA3.1 backbone. Cycloheximide (2112S, Cell Signaling Technology, Danvers, MA) was used to evaluate the stability and half-life of the protein. Apoptosis was induced by treating cells with the nonspecific kinase inhibitor staurosporine (S5921, MilliporeSigma, St. Louis, MO). All primer and restriction enzyme information used for plasmid construct cloning can be found in Table S2.

Cycloheximide Chase. To analyze the protein half-life via cycloheximide chase, 5.0×10^5 HEK 293T cells were cultured in 6-well plates and transfected with 1 μg of either pcDNA3.1-PACS2(WT)-FLAG or pcDNA3.1-PACS2(E209K)-FLAG. All transfections used 3 μL of the PolyJet transfection reagent (SignaGen, Rockville, MD) per well. Twenty-four hours post-transfection, morphologically equivalent cells were treated with 50 ng/μL cycloheximide for periods of 0, 1, 2, 3, 4, 8, or 12 h. After the incubation of cycloheximide, cells were scraped into Eppendorf tubes and then centrifuged to remove cycloheximide-containing DMEM. Cells were washed twice with 1× PBS, scraped, and lysed with 1× lysis buffer (25 mM HEPES, 300 mM NaCl, 1.5 mM $MgCl_2$, 0.2 mM EDTA, and 0.1% Triton X-100) containing a protease inhibitor cocktail (Roche, Basel, Switzerland) and a phosphatase inhibitor (10 mM NaF and 10 mM Na_3VO_4) at 4 °C for 30 min with rocking. Collected cell lysates were resuspended in 5× SDS loading buffer (0.25 M tris-HCl, pH 6.8; 0.25% bromophenol blue; 10% SDS; 15% β-mercaptoethanol; and 50% glycerol), boiled at 98 °C for 10 min, and stored at −20 °C before Western blot analysis.

Cross-Linking with 1,4-Bismaleimidobutane (BMB). For protein oligomerization experiments, 5.0×10^5 HEK 293T cells were cultured in 6-well plates and transfected with 1 μg of either pcDNA3.1-PACS2(WT)-FLAG or pcDNA3.1-PACS2-(E209K)-FLAG. All transfections used 3 μL of the PolyJet transfection reagent per well. Twenty-four hours post-transfection, cells were washed with 1× PBS and incubated in either 1% DMSO or 200 μM BMB (dissolved in 1× PBS) for 1 h. After being cross-linked with BMB, cells were scraped into Eppendorf tubes and then centrifuged to remove BMB-containing 1× PBS. Cells were washed twice with 5 mM cysteine dissolved in 1× PBS (quenching solution) and lysed with 1× lysis buffer (25 mM HEPES, 300 mM NaCl, 1.5 mM $MgCl_2$, 0.2 mM EDTA, and 0.1% Triton X-100) containing a protease inhibitor cocktail (Roche, Basel, Switzerland) and a phosphatase inhibitor (10 mM NaF and 10 mM Na_3VO_4) at 4 °C for 30 min with rocking. Collected cell lysates were resuspended in 5× SDS loading buffer, boiled at 98 °C for 10 min, and stored at −20 °C before Western blot analysis.

Co-Immunoprecipitation (coIPs). For the coimmunoprecipitation of PACS-2 WT and E209K with 14-3-3ε, 2.0×10^6 HEK 293T cells were cultured in 10 cm dishes and either transfected with 2.5 μg of pIRES-14-3-3ε-HA-IRES-14-3-3ζ-myc or cotransfected with 2.5 μg each of pIRES-14-3-3ε-HA-IRES-14-3-3ζ-myc and either pcDNA3.1-PACS2(WT)-FLAG or pcDNA3.1-PACS2(E209K)-FLAG. All transfections used 15 μLof the PolyJet transfection reagent per dish. Twenty-four hours post-transfection, cells were washed twice with cold PBS. Cells were then treated with 1× lysis buffer (1.5 mM $MgCl_2$; 1 mM EGTA; 50 mM HEPES, pH 7.4; 150 mM NaCl; 1% Triton X-100; and 10% glycerol) supplemented with 1 mM NaF, 2 mM Na_3VO_4, and a protease inhibitor cocktail (Roche) and rocked for 30 min at 4 °C. After 30 min, cells were scraped and left to rock for another 30 min at 4 °C. The lysed cells were centrifuged at 21,000*g* for 30 min at 4 °C. For use as the input control, 50 μL of the supernatant containing the cell lysate was resuspended in 5× SDS loading buffer, boiled at 98 °C for 10 min, and stored at −20 °C. The remaining cell lysate was incubated overnight at 4 °C with 30 μL of anti-DYKDDDDK tag (L5) affinity gel (BioLegend, San Diego, CA). The next day, the affinity gel was washed with the wash buffer (700 μL/wash of 1× PBS, four washes, 5 min/wash), resuspended in the 5× SDS loading buffer, boiled at 98 °C for 10 min, and stored at −20 °C prior to Western blot analysis. To normalize the co-IP results, immunoprecipitated 14-3-3ε was normalized to the sum of the amount of PACS-2 IP and the amount of 14-3-3ε in the input.

Expression of Transfected Constructs. To measure the expression of exogenous and endogenous proteins, 5.0×10^5 HEK 293T cells were cultured in 6-well plates and transfected with 1 μg of either pcDNA3.1-PACS2(WT)-FLAG or pcDNA3.1-PACS2(E209K)-FLAG. In addition, 5.0×10^5 HCT116 cells were cultured in 6-well plates and transfected with 1 μg of pIRES-14-3-3ε-IRES-eGFP, pIRES-PACS2(WT)-FLAG-IRES-eGFP, or pIRES-PACS(E209K)-FLAG-IRES-eGFP. All transfections used 3 μL of the PolyJet transfection reagent per dish. Thirty hours post-transfection, cells were washed twice with 1× PBS, scraped, and lysed with 1× lysis buffer (25 mM HEPES, 300 mM NaCl, 1.5 mM $MgCl_2$, 0.2 mM EDTA, and 0.1% Triton X-100) containing a protease inhibitor cocktail (Roche) and a phosphatase inhibitor (10 mM NaF and 10 mM Na_3VO_4) at 4 °C for 30 min with rocking. Collected cell lysates were resuspended in the 5× SDS loading buffer, boiled at 98 °C for 10 min, and stored at −20 °C before Western blot analysis.

Western Blot. Equal amounts of boiled cell lysates from HEK 293T cells or HCT116 cells were loaded onto SDS polyacrylamide gels and subjected to SDS-PAGE. Gels were run at 80 V for 30 min, followed by 120 V for 1 h 30 min, then transferred to Amersham Protran 0.45 μm nitrocellulose membranes (GE Healthcare, Boston, MA) in transfer buffer (25 mM tris-HCl; 192 mM glycine, pH 8.3; and 20% methanol) at 320 mA for 3 h. Membranes were blocked in tris-buffered saline Tween 20 (TBST) buffer (150 mM NaCl; 10 mM tris-HCl, pH 8.0; and 0.1% Tween 20) with 5% nonfat skim milk (BioShop, Burlington, ON) for 45 min before overnight incubation with primary antibodies at 4 °C. Anti-FLAG (BioLegend, 637303; WB from 1:10 000 to 1:20 000), anti-HA (MilliporeSigma, H6908; WB 1:1000), and anti-β-actin (Invitrogen, Carlsbad, CA, MA1-744; WB 1:5000) were used as primary antibodies. After primary staining, membranes were washed thrice with 1× TBST for 5 min each and then incubated with a secondary antibody (the same concentration as the primary antibodies) at room temperature for 1 h. Antirabbit IgG (H+L) HRP (Invitrogen; WB 1:3000), antirat IgG (H + L) HRP (Invitrogen; WB 1:20000), and antimouse IgG (H + L) HRP (Invitrogen; WB 1:5000) were used as secondary antibodies. Postincubation, membranes were washed thrice with 1× TBST for 5 min each; subjected to

https://doi.org/10.1021/acsomega.2c04014
ACS Omega 2022, 7, 34378−34388

an HRP reaction with the Pierce ECL (Thermo Scientific, Waltham, MA), Classico, or Forte substrate (MilliporeSigma); and imaged with a C-DiGit chemiluminescence scanner (LI-COR Biosciences, Lincoln, NE).

Flow Cytometry for the Analysis of Staurosporine-Induced Apoptosis. To evaluate the expression of various constructs on staurosporine-induced apoptosis, 5.0×10^5 HCT116 cells were cultured in 6-well plates and transfected with either 2 μg of pN1-eGFP as a single-stained GFP-expressing gating control or 1 μg pBJ5-empty as an unstained control. Furthermore, cells were transfected with 1 μg of pN1-eGFP, pIRES-14-3-3ε-HA-IRES-eGFP, pIRES-PACS2(WT)-FLAG-IRES-eGFP, or pIRES-PACS2(E209K)-FLAG-IRES-eGFP. All transfections used 3 μL of the PolyJet transfection reagent per well. Twenty-four hours post-transfection, the experimental cells were treated with 1 μM staurosporine for 6 h, while the control cells used to gate positive apoptosis signals were treated with 2 μM staurosporine for 6 h. After the staurosporine treatment, transfected HCT116 cells were harvested from 6-well plates with trypsin-EDTA (25300054, Thermo Scientific) into polystyrene tubes. Cells were spun down at room temperature and washed thrice with 1× PBS. Cells were subjected to viability staining with the Pacific Blue Annexin V Apoptosis Detection Kit with 7-AAD (640926, BioLegend) following the manufacturer's recommendations. Stained cells were analyzed immediately via flow cytometry using the FACSCanto SORP (BD Biosciences) system without fixation. The whole-cell population was used for analysis to ensure the inclusion of apoptotic and surviving cells. An eGFP fluorescence gate was identified based on a comparison of the bright (2 μg of DNA) cells transfected with pN1-eGFP and the unstained cells transfected with pBJ5-empty. The fluorescence minus one (FMO) samples included three populations stained with the dual-color recombination of eGFP, 7-AAD, or Pacific Blue Annexin V to identify the 7-AAD$^+$ and Annexin V$^+$ cells (Figure S5). Mean fluorescence intensities (MFI) of GFP within GFP$^+$ cells were quantified as a proxy measurement for 14-3-3ε, PACS-2 WT, and PACS-2 E209K expression within the transfected GFP$^+$ cells treated with either DMSO or staurosporine (Figure S6).

Statistical Tests. Statistical analysis was performed with GraphPad Prism ver. 8.0 software (GraphPad Software, San Diego, CA). The statistical significance between two groups was determined using an unpaired two-tailed Student's *t*-test assuming equal variance with a 95% confidence interval (α = 0.05). Statistical significance including three or more groups was determined using a nonmatching one-way analysis of variance (ANOVA) test, followed by a Holm−Šidák multiple-comparison test with a 95% confidence interval (α = 0.05). The statistical analysis shown in Figure S6 utilized a one-way ANOVA test, followed by a Tukey multiple-comparison test with a 95% confidence interval (α = 0.05).

■ ASSOCIATED CONTENT

Supporting Information

The Supporting Information is available free of charge at https://pubs.acs.org/doi/10.1021/acsomega.2c04014.

Additional information on the predicted PACS-2 E209K protein structure; supporting data on protein expression, construct design, FACS gating, and MFI measurements of GFP; PACS-2 sequences used for analysis; and oligonucleotides used for molecular cloning (PDF)

Accession Codes

UniProt accession IDs for proteins used in this study are Q86VP3 for PACS-2 and P62258 for 14-3-3ε.

■ AUTHOR INFORMATION

Corresponding Author

Jimmy D. Dikeakos − *Department of Microbiology and Immunology, The University of Western Ontario, Schulich School of Medicine and Dentistry, London, ON N6A 5C1, Canada;* orcid.org/0000-0001-8141-5395; Email: jimmy.dikeakos@uwo.ca

Authors

Rong Xuan Zang − *Department of Microbiology and Immunology, The University of Western Ontario, Schulich School of Medicine and Dentistry, London, ON N6A 5C1, Canada*

Mitchell J. Mumby − *Department of Microbiology and Immunology, The University of Western Ontario, Schulich School of Medicine and Dentistry, London, ON N6A 5C1, Canada*

Complete contact information is available at: https://pubs.acs.org/10.1021/acsomega.2c04014

Author Contributions

M.J.M., R.X.Z., and J.D.D. designed the research; R.X.Z. conducted the experimental research; R.X.Z and M.J.M. analyzed data; R.X.Z. wrote the paper with feedback from M.J.M. and J.D.D.; and J.D.D. supervised the project.

Funding

This work was funded by a Discovery Grant from the Natural Sciences and Engineering Council of Canada to J.D.D. (no. 04094). R.X.Z. and M.M.M. were partially supported by an Ontario Graduate Studentship from the Government of Ontario. R.X.Z. is currently supported by a Natural Sciences and Engineering Research Council Canadian Graduate Scholarship Masters from the Government of Canada.

Notes

The authors declare no competing financial interest.

■ ACKNOWLEDGMENTS

BioRender was utilized to make the table of content graphics with an academic license for journal publication (agreement no. SB245UPTML).

■ ABBREVIATIONS

Akt, protein kinase B; Bid, BH3 interacting-domain death agonist; BMB, 1,4-bismaleimidobutane; CHX, cycloheximide; CTR, C-terminal region; FBR, furin binding region; HDAC1, histone deacetylase 1; IRES, internal ribosomal entry site; MFI, mean fluorescence intensity; MR, middle region; NLS, nuclear localization signal; PACS-2, phosphofurin acidic cluster sorting protein 2; SIRT1, sirtuin 1; TRAIL, tumor necrosis factor-related apoptosis-inducing ligand; TRPV1, transient receptor potential cation channel subfamily V member 1

■ REFERENCES

(1) Dombernowsky, S. L.; Samsøe-Petersen, J.; Petersen, C. H.; Instrell, R.; Hedegaard, A.-M. B.; Thomas, L.; Atkins, K. M.; Auclair, S.; Albrechtsen, R.; Mygind, K. J.; Fröhlich, C.; Howell, M.; Parker, P.; Thomas, G.; Kveiborg, M. The Sorting Protein PACS-2 Promotes ErbB Signalling by Regulating Recycling of the Metalloproteinase ADAM17. *Nat. Commun.* **2015**, *6*, 7518.

(2) Werneburg, N. W.; Bronk, S. F.; Guicciardi, M. E.; Thomas, L.; Dikeakos, J. D.; Thomas, G.; Gores, G. J. Tumor Necrosis Factor-Related Apoptosis-Inducing Ligand (TRAIL) Protein-Induced Lysosomal Translocation of Proapoptotic Effectors Is Mediated by Phosphofurin Acidic Cluster Sorting Protein-2 (PACS-2). *J. Biol. Chem.* **2012**, *287* (29), 24427−24437.
(3) Simmen, T.; Aslan, J. E.; Blagoveshchenskaya, A. D.; Thomas, L.; Wan, L.; Xiang, Y.; Feliciangeli, S. F.; Hung, C. H.; Crump, C. M.; Thomas, G. PACS-2 Controls Endoplasmic Reticulum-Mitochondria Communication and Bid-Mediated Apoptosis. *EMBO J.* **2005**, *24* (4), 717−729.
(4) Köttgen, M.; Benzing, T.; Simmen, T.; Tauber, R.; Buchholz, B.; Feliciangeli, S.; Huber, T. B.; Schermer, B.; Kramer-Zucker, A.; Höpker, K.; Simmen, K. C.; Tschucke, C. C.; Sandford, R.; Kim, E.; Thomas, G.; Walz, G. Trafficking of TRPP2 by PACS Proteins Represents a Novel Mechanism of Ion Channel Regulation. *EMBO J.* **2005**, *24* (4), 705−716.
(5) Myhill, N.; Lynes, E. M.; Nanji, J. A.; Blagoveshchenskaya, A. D.; Fei, H.; Carmine Simmen, K.; Cooper, T. J.; Thomas, G.; Simmen, T. The Subcellular Distribution of Calnexin Is Mediated by PACS-2. *Mol. Biol. Cell* **2008**, *19* (7), 2777−2788.
(6) Feliciangeli, S. F.; Thomas, L.; Scott, G. K.; Subbian, E.; Hung, C.-H.; Molloy, S. S.; Jean, F.; Shinde, U.; Thomas, G. Identification of a PH Sensor in the Furin Propeptide That Regulates Enzyme Activation. *J. Biol. Chem.* **2006**, *281* (23), 16108−16116.
(7) Youker, R. T.; Shinde, U.; Day, R.; Thomas, G. At the Crossroads of Homoeostasis and Disease: Roles of the PACS Proteins in Membrane Traffic and Apoptosis. *Biochem. J.* **2009**, *421*, 1−15.
(8) Thomas, G.; Aslan, J. E.; Thomas, L.; Shinde, P.; Shinde, U.; Simmen, T. Caught in the Act -Protein Adaptation and the Expanding Roles of the PACS Proteins in Tissue Homeostasis and Disease. *J. Cell Sci.* **2017**, *130* (11), 1865−1876.
(9) Hornbeck, P. V.; Zhang, B.; Murray, B.; Kornhauser, J. M.; Latham, V.; Skrzypek, E. PhosphoSitePlus, 2014: Mutations, PTMs and Recalibrations. *Nucleic Acids Res.* **2015**, *43* (D1), D512−D520.
(10) Atkins, K. M.; Thomas, L. L.; Barroso-Gonzalez, J.; Thomas, L.; Auclair, S.; Yin, J.; Kang, H.; Chung, J. H.; Dikeakos, J. D.; Thomas, G. The Multifunctional Sorting Protein PACS-2 Regulates SIRT1-Mediated Deacetylation of P53 to Modulate P21-Dependent Cell-Cycle Arrest. *Cell Rep.* **2014**, *8* (5), 1545−1557.
(11) Krzysiak, T. C.; Thomas, L.; Choi, Y. J.; Auclair, S.; Qian, Y.; Luan, S.; Krasnow, S. M.; Thomas, L. L.; Koharudin, L. M. I.; Benos, P. V.; Marks, D. L.; Gronenborn, A. M.; Thomas, G. An Insulin-Responsive Sensor in the SIRT1 Disordered Region Binds DBC1 and PACS-2 to Control Enzyme Activity. *Mol. Cell* **2018**, *72* (6), 985−998.
(12) Aslan, J. E.; You, H.; Williamson, D. M.; Endig, J.; Youker, R. T.; Thomas, L.; Shu, H.; Du, Y.; Milewski, R. L.; Brush, M. H.; Possemato, A.; Sprott, K.; Fu, H.; Greis, K. D.; Runckel, D. N.; Vogel, A.; Thomas, G. Akt and 14−3-3 Control a PACS-2 Homeostatic Switch That Integrates Membrane Traffic with TRAIL-Induced Apoptosis. *Mol. Cell* **2009**, *34* (4), 497−509.
(13) Betz, C.; Stracka, D.; Prescianotto-Baschong, C.; Frieden, M.; Demaurex, N.; Hall, M. N. MTOR Complex 2-Akt Signaling at Mitochondria-Associated Endoplasmic Reticulum Membranes (MAM) Regulates Mitochondrial Physiology. *Proc. Natl. Acad. Sci. U. S. A.* **2013**, *110* (31), 12526−12534.
(14) Olson, H. E.; Jean-Marçais, N.; Yang, E.; Heron, D.; Tatton-Brown, K.; van der Zwaag, P. A.; Bijlsma, E. K.; Krock, B. L.; Backer, E.; Kamsteeg, E. J.; Sinnema, M.; Reijnders, M. R. F.; Bearden, D.; Begtrup, A.; Telegrafi, A.; Lunsing, R. J.; Burglen, L.; Lesca, G.; Cho, M. T.; Smith, L. A.; Sheidley, B. R.; Moufawad El Achkar, C.; Pearl, P. L.; Poduri, A.; Skraban, C. M.; Tarpinian, J.; Nesbitt, A. I.; Fransen van de Putte, D. E.; Ruivenkamp, C. A. L.; Rump, P.; Chatron, N.; Sabatier, I.; De Bellescize, J.; Guibaud, L.; Sweetser, D. A.; Waxler, J. L.; Wierenga, K. J.; Donadieu, J.; Narayanan, V.; Ramsey, K. M.; Nava, C.; Rivière, J. B.; Vitobello, A.; Tran Mau-Them, F.; Philippe, C.; Bruel, A. L.; Duffourd, Y.; Thomas, L.; Lelieveld, S. H.; Schuurs-Hoeijmakers, J.; Brunner, H. G.; Keren, B.; Thevenon, J.; Faivre, L.; Thomas, G.; Thauvin-Robinet, C. A Recurrent De Novo PACS2 Heterozygous Missense Variant Causes Neonatal-Onset Developmental Epileptic Encephalopathy, Facial Dysmorphism, and Cerebellar Dysgenesis. *Am. J. Hum. Genet.* **2018**, *102* (5), 995−1007.
(15) Terrone, G.; Marchese, F.; Vari, M. S.; Severino, M.; Madia, F.; Amadori, E.; Del Giudice, E.; Romano, A.; Gennaro, E.; Zara, F.; Striano, P. A Further Contribution to the Delineation of Epileptic Phenotype in PACS2-Related Syndrome. *Seizure* **2020**, *79*, 53−55.
(16) Mizuno, T.; Miyata, R.; Hojo, A.; Tamura, Y.; Nakashima, M.; Mizuguchi, T.; Matsumoto, N.; Kato, M. Clinical Variations of Epileptic Syndrome Associated with PACS2 Variant. *Brain Dev.* **2021**, *43*, 343−347.
(17) Sakaguchi, Y.; Yoshihashi, H.; Uehara, T.; Miyama, S.; Kosaki, K.; Takenouchi, T. Coloboma May Be a Shared Feature in a Spectrum of Disorders Caused by Mutations in the WDR37-PACS1-PACS2 Axis. *Am. J. Med. Genet. A* **2021**, *185* (3), 884−888.
(18) Sánchez-Soler, M. J.; Serrano-Antón, A. T.; López-González, V.; Guillén-Navarro, E. New Case with the Recurrent c.625G>A Pathogenic Variant in the PACS2 Gene: Expanding the Phenotype. *Neurologia* **2021**, *36* (9), 716−719.
(19) Xiao, T. T.; Yang, L.; Wu, B. B.; Peng, X. M.; Wang, H. J.; Cheng, G. Q.; Wang, L. S.; Cao, Y.; Hu, L. Y.; Zhou, W. H. Genotype and phenotype analysis of neonates with neonatal encephalopathy complicated with perinatal hypoxic event. *Chin. J. Pediatr.* **2021**, *59* (4), 280−285.
(20) Wu, M. J.; Hu, C. H.; Ma, J. H.; Hu, J. S.; Liu, Z. S.; Sun, D. Early infantile epileptic encephalopathy caused by PACS2 gene mutation and literature review. *Chin. J. Pediatr.* **2021**, *59* (7), 594−599.
(21) Shen, Y.; Li, Y.; Zhang, J.; Yuan, M.; Zhang, J.; Luo, R.; Gan, J. Clinical and genetic analysis of PACS2 gene mutation in two child patients with developmental and epileptic encephalopathy 66. *Chin. J. Med. Genet.* **2021**, *38* (10), 969−972.
(22) Valenzuela, I.; Guillén Benítez, E.; Sanchez-Montanez, A.; Limeres, J.; López-Grondona, F.; Cuscó, I.; Tizzano, E. F. Vein of Galen Aneurysm, Dilated Cardiomyopathy, and Slender Habitus in a Patient with a Recurrent Pathogenic Variant in PACS2. *Am. J. Med. Genet. A* **2022**, *188* (3), 991−995.
(23) Cesaroni, E.; Matricardi, S.; Cappanera, S.; Marini, C. First Reported Case of an Inherited PACS2 Pathogenic Variant with Variable Expression. *Epileptic Disord.* **2022**, *24*, 572.
(24) Sayers, E. W.; Bolton, E. E.; Brister, J. R.; Canese, K.; Chan, J.; Comeau, D. C.; Connor, R.; Funk, K.; Kelly, C.; Kim, S.; Madej, T.; Marchler-Bauer, A.; Lanczycki, C.; Lathrop, S.; Lu, Z.; Thibaud-Nissen, F.; Murphy, T.; Phan, L.; Skripchenko, Y.; Tse, T.; Wang, J.; Williams, R.; Trawick, B. W.; Pruitt, K. D.; Sherry, S. T. Database Resources of the National Center for Biotechnology Information. *Nucleic Acids Res.* **2022**, *50* (D1), D20−D26.
(25) Jumper, J.; Evans, R.; Pritzel, A.; Green, T.; Figurnov, M.; Ronneberger, O.; Tunyasuvunakool, K.; Bates, R.; Žídek, A.; Potapenko, A.; Bridgland, A.; Meyer, C.; Kohl, S. A. A.; Ballard, A. J.; Cowie, A.; Romera-Paredes, B.; Nikolov, S.; Jain, R.; Adler, J.; Back, T.; Petersen, S.; Reiman, D.; Clancy, E.; Zielinski, M.; Steinegger, M.; Pacholska, M.; Berghammer, T.; Bodenstein, S.; Silver, D.; Vinyals, O.; Senior, A. W.; Kavukcuoglu, K.; Kohli, P.; Hassabis, D. Highly Accurate Protein Structure Prediction with AlphaFold. *Nature* **2021**, *596* (7873), 583−589.
(26) Varadi, M.; Anyango, S.; Deshpande, M.; Nair, S.; Natassia, C.; Yordanova, G.; Yuan, D.; Stroe, O.; Wood, G.; Laydon, A.; Žídek, A.; Green, T.; Tunyasuvunakool, K.; Petersen, S.; Jumper, J.; Clancy, E.; Green, R.; Vora, A.; Lutfi, M.; Figurnov, M.; Cowie, A.; Hobbs, N.; Kohli, P.; Kleywegt, G.; Birney, E.; Hassabis, D.; Velankar, S. AlphaFold Protein Structure Database: Massively Expanding the Structural Coverage of Protein-Sequence Space with High-Accuracy Models. *Nucleic Acids Res.* **2022**, *50* (D1), D439−D444.
(27) Cortese, M. S.; Uversky, V. N.; Dunker, A. K. Intrinsic Disorder in Scaffold Proteins: Getting More from Less. *Prog. Biophys. Mol. Biol.* **2008**, *98* (1), 85−106.

https://doi.org/10.1021/acsomega.2c04014
ACS Omega 2022, 7, 34378−34388

(28) Schuurs-Hoeijmakers, J. H. M.; Landsverk, M. L.; Foulds, N.; Kukolich, M. K.; Gavrilova, R. H.; Greville-Heygate, S.; Hanson-Kahn, A.; Bernstein, J. A.; Glass, J.; Chitayat, D.; Burrow, T. A.; Husami, A.; Collins, K.; Wusik, K.; van der Aa, N.; Kooy, F.; Brown, K. T.; Gadzicki, D.; Kini, U.; Alvarez, S.; Fernández-Jaén, A.; Mcgehee, F.; Selby, K.; Tarailo-Graovac, M.; Van Allen, M.; van Karnebeek, C. D. M.; Stavropoulos, D. J.; Marshall, C. R.; Merico, D.; Gregor, A.; Zweier, C.; Hopkin, R. J.; Chu, Y. W. Y.; Chung, B. H. Y.; de Vries, B. B. A.; Devriendt, K.; Hurles, M. E.; Brunner, H. G. Clinical Delineation of the PACS1-Related Syndrome-Report on 19 Patients. *Am. J. Med. Genet. Part A* **2016**, *170* (3), 670−675.
(29) Schuurs-Hoeijmakers, J. H. M.; Oh, E. C.; Vissers, L. E. L. M.; Swinkels, M. E. M.; Gilissen, C.; Willemsen, M. A.; Holvoet, M.; Steehouwer, M.; Veltman, J. A.; De Vries, B. B. A.; Van Bokhoven, H.; De Brouwer, A. P. M.; Katsanis, N.; Devriendt, K.; Brunner, H. G. Recurrent de Novo Mutations in PACS1 Cause Defective Cranial-Neural-Crest Migration and Define a Recognizable Intellectual-Disability Syndrome. *Am. J. Hum. Genet.* **2012**, *91* (6), 1122−1127.
(30) Uversky, V. N. Intrinsically Disordered Proteins and Their (Disordered) Proteomes in Neurodegenerative Disorders. *Front. Aging Neurosci.* **2015**, *7*, 18.
(31) Uversky, V. N.; Oldfield, C. J.; Dunker, A. K. Showing Your ID: Intrinsic Disorder as an ID for Recognition, Regulation and Cell Signaling. *J. Mol. Recognit.* **2005**, *18* (5), 343−384.
(32) Hedskog, L.; Pinho, C. M.; Filadi, R.; Rönnbäck, A.; Hertwig, L.; Wiehager, B.; Larssen, P.; Gellhaar, S.; Sandebring, A.; Westerlund, M.; Graff, C.; Winblad, B.; Galter, D.; Behbahani, H.; Pizzo, P.; Glaser, E.; Ankarcrona, M. Modulation of the Endoplasmic Reticulum-Mitochondria Interface in Alzheimer's Disease and Related Models. *Proc. Natl. Acad. Sci. U. S. A.* **2013**, *110* (19), 7916−7921.
(33) Mallik, S.; Kundu, S. Topology and Oligomerization of Mono- and Oligomeric Proteins Regulate Their Half-Lives in the Cell. *Structure* **2018**, *26* (6), 869−878.
(34) Choi, M. L.; Gandhi, S. Crucial Role of Protein Oligomerization in the Pathogenesis of Alzheimer's and Parkinson's Diseases. *FEBS J.* **2018**, *285* (19), 3631−3644.
(35) Schneider, B.; Baudry, A.; Pietri, M.; Alleaume-Butaux, A.; Bizingre, C.; Nioche, P.; Kellermann, O.; Launay, J.-M. The Cellular Prion Protein-ROCK Connection: Contribution to Neuronal Homeostasis and Neurodegenerative Diseases. *Front. Cell. Neurosci.* **2021**, *15*, 660683.
(36) Ross, C. A.; Poirier, M. A. Protein Aggregation and Neurodegenerative Disease. *Nat. Med.* **2004**, *10* (Suppl), S10−7.
(37) Thibaudeau, T. A.; Anderson, R. T.; Smith, D. M. A Common Mechanism of Proteasome Impairment by Neurodegenerative Disease-Associated Oligomers. *Nat. Commun.* **2018**, *9* (1), 1097.
(38) Guicciardi, M. E.; Werneburg, N. W.; Bronk, S. F.; Franke, A.; Yagita, H.; Thomas, G.; Gores, G. J. Cellular Inhibitor of Apoptosis (CIAP)-Mediated Ubiquitination of Phosphofurin Acidic Cluster Sorting Protein 2 (PACS-2) Negatively Regulates Tumor Necrosis Factor-Related Apoptosis-Inducing Ligand (TRAIL) Cytotoxicity. *PLoS One* **2014**, *9* (3), No. e92124.
(39) Ingelsson, M. Alpha-Synuclein Oligomers-Neurotoxic Molecules in Parkinson's Disease and Other Lewy Body Disorders. *Front. Neurosci.* **2016**, *10*, 408.
(40) Hallacli, E.; Kayatekin, C.; Nazeen, S.; Wang, X. H.; Sheinkopf, Z.; Sathyakumar, S.; Sarkar, S.; Jiang, X.; Dong, X.; Di Maio, R.; Wang, W.; Keeney, M. T.; Felsky, D.; Sandoe, J.; Vahdatshoar, A.; Udeshi, N. D.; Mani, D. R.; Carr, S. A.; Lindquist, S.; De Jager, P. L.; Bartel, D. P.; Myers, C. L.; Greenamyre, J. T.; Feany, M. B.; Sunyaev, S. R.; Chung, C. Y.; Khurana, V. The Parkinson's Disease Protein Alpha-Synuclein Is a Modulator of Processing Bodies and MRNA Stability. *Cell* **2022**, *185* (12), 2035−2056.
(41) Costa-Mattioli, M.; Monteggia, L. M. MTOR Complexes in Neurodevelopmental and Neuropsychiatric Disorders. *Nat. Neurosci.* **2013**, *16* (11), 1537−1543.
(42) Cornell, B.; Toyo-oka, K. 14-3-3 Proteins in Brain Development: Neurogenesis, Neuronal Migration and Neuromorphogenesis. *Front. Mol. Neurosci.* **2017**, *10*, 318.
(43) Toyo-Oka, K.; Wachi, T.; Hunt, R. F.; Baraban, S. C.; Taya, S.; Ramshaw, H.; Kaibuchi, K.; Schwarz, Q. P.; Lopez, A. F.; Wynshaw-Boris, A. 14−3-3ε and ζ Regulate Neurogenesis and Differentiation of Neuronal Progenitor Cells in the Developing Brain. *J. Neurosci.* **2014**, *34* (36), 12168−12181.
(44) Yamaguchi, Y.; Miura, M. Programmed Cell Death in Neurodevelopment. *Dev. Cell* **2015**, *32* (4), 478−490.
(45) Ahuja, D.; Sáenz-Robles, M. T.; Pipas, J. M. SV40 Large T Antigen Targets Multiple Cellular Pathways to Elicit Cellular Transformation. *Oncogene* **2005**, *24* (52), 7729−7745.
(46) Holmes, T. R.; Al Matouq, J.; Holmes, M.; Sioda, N.; Rudd, J. C.; Bloom, C.; Nicola, L.; Palermo, N. Y.; Madson, J. G.; Lovas, S.; Hansen, L. A. Targeting 14−3-3ε Activates Apoptotic Signaling to Prevent Cutaneous Squamous Cell Carcinoma. *Carcinogenesis* **2021**, *42* (2), 232−242.
(47) Qiu, Y.; Zhou, Z.; Li, Z.; Lu, L.; Li, L.; Li, X.; Wang, X.; Zhang, M. Pretreatment 14−3-3 Epsilon Level Is Predictive for Advanced Extranodal NK/T Cell Lymphoma Therapeutic Response to Asparaginase-Based Chemotherapy. *Prot. Clin. Appl.* **2017**, *11* (3−4), No. 1600111.
(48) Liu, T.-A.; Jan, Y.-J.; Ko, B.-S.; Liang, S.-M.; Chen, S.-C.; Wang, J.; Hsu, C.; Wu, Y.-M.; Liou, J.-Y. 14−3-3ε Overexpression Contributes to Epithelial-Mesenchymal Transition of Hepatocellular Carcinoma. *PLoS One* **2013**, *8* (3), e57968.
(49) Chuthapisith, S.; Layfield, R.; Kerr, I. D.; Hughes, C.; Eremin, O. Proteomic Profiling of MCF-7 Breast Cancer Cells with Chemoresistance to Different Types of Anti-Cancer Drugs. *Int. J. Oncol.* **2007**, *30* (6), 1545−1551.
(50) Liou, J.-Y.; Ghelani, D.; Yeh, S.; Wu, K. K. Nonsteroidal Anti-Inflammatory Drugs Induce Colorectal Cancer Cell Apoptosis by Suppressing 14−3-3epsilon. *Cancer Res.* **2007**, *67* (7), 3185−3191.
(51) Masters, S. C.; Fu, H. 14−3-3 Proteins Mediate an Essential Anti-Apoptotic Signal. *J. Biol. Chem.* **2001**, *276* (48), 45193−45200.
(52) Simmen, T.; Aslan, J. E.; Blagoveshchenskaya, A. D.; Thomas, L.; Wan, L.; Xiang, Y.; Feliciangeli, S. F.; Hung, C. H.; Crump, C. M.; Thomas, G. PACS-2 Controls Endoplasmic Reticulum-Mitochondria Communication and Bid-Mediated Apoptosis. *EMBO J.* **2005**, *24* (4), 717−729.
(53) Karaman, M. W.; Herrgard, S.; Treiber, D. K.; Gallant, P.; Atteridge, C. E.; Campbell, B. T.; Chan, K. W.; Ciceri, P.; Davis, M. I.; Edeen, P. T.; Faraoni, R.; Floyd, M.; Hunt, J. P.; Lockhart, D. J.; Milanov, Z. V.; Morrison, M. J.; Pallares, G.; Patel, H. K.; Pritchard, S.; Wodicka, L. M.; Zarrinkar, P. P. A Quantitative Analysis of Kinase Inhibitor Selectivity. *Nat. Biotechnol.* **2008**, *26* (1), 127−132.
(54) Du, X.; Fox, J. E.; Pei, S. Identification of a Binding Sequence for the 14−3-3 Protein within the Cytoplasmic Domain of the Adhesion Receptor, Platelet Glycoprotein Ib Alpha. *J. Biol. Chem.* **1996**, *271* (13), 7362−7367.
(55) Petosa, C.; Masters, S. C.; Bankston, L. A.; Pohl, J.; Wang, B.; Fu, H.; Liddington, R. C. 14−3-3zeta Binds a Phosphorylated Raf Peptide and an Unphosphorylated Peptide via Its Conserved Amphipathic Groove. *J. Biol. Chem.* **1998**, *273* (26), 16305−16310.
(56) Shinoda, S.; Schindler, C. K.; Quan-Lan, J.; Saugstad, J. A.; Taki, W.; Simon, R. P.; Henshall, D. C. Interaction of 14−3-3 with Bid during Seizure-Induced Neuronal Death. *J. Neurochem.* **2003**, *86* (2), 460−469.
(57) Barroso-González, J.; Auclair, S.; Luan, S.; Thomas, L.; Atkins, K. M.; Aslan, J. E.; Thomas, L. L.; Zhao, J.; Zhao, Y.; Thomas, G. PACS-2 Mediates the ATM and NF-$κ$B-Dependent Induction of Anti-Apoptotic Bcl-XL in Response to DNA Damage. *Cell Death Differ.* **2016**, *23* (9), 1448−1457.
(58) Knoell, J.; Chillappagari, S.; Knudsen, L.; Korfei, M.; Dartsch, R.; Jonigk, D.; Kuehnel, M. P.; Hoetzenecker, K.; Guenther, A.; Mahavadi, P. PACS2-TRPV1 Axis Is Required for ER-Mitochondrial Tethering during ER Stress and Lung Fibrosis. *Cell. Mol. Life Sci.* **2022**, *79* (3), 151.
(59) Short, D. M.; Heron, I. D.; Birse-Archbold, J.-L. A.; Kerr, L. E.; Sharkey, J.; McCulloch, J. Apoptosis Induced by Staurosporine Alters

https://doi.org/10.1021/acsomega.2c04014
ACS Omega 2022, 7, 34378−34388

Chaperone and Endoplasmic Reticulum Proteins: Identification by Quantitative Proteomics. *Proteomics* **2007**, *7* (17), 3085−3096.
(60) Blanquie, O.; Kilb, W.; Sinning, A.; Luhmann, H. J. Homeostatic Interplay between Electrical Activity and Neuronal Apoptosis in the Developing Neocortex. *Neuroscience* **2017**, *358*, 190−200.
(61) Cocito, C.; Merighi, A.; Giacobini, M.; Lossi, L. Alterations of Cell Proliferation and Apoptosis in the Hypoplastic Reeler Cerebellum. *Front. Cell. Neurosci.* **2016**, *10*, 141.
(62) Suzanne, M.; Steller, H. Shaping Organisms with Apoptosis. *Cell Death Differ.* **2013**, *20* (5), 669−675.
(63) Ku, C. S.; Polychronakos, C.; Tan, E. K.; Naidoo, N.; Pawitan, Y.; Roukos, D. H.; Mort, M.; Cooper, D. N. A New Paradigm Emerges from the Study of de Novo Mutations in the Context of Neurodevelopmental Disease. *Mol. Psychiatry* **2013**, *18* (2), 141−153.
(64) Deciphering Developmental Disorders Study. Prevalence and Architecture of de Novo Mutations in Developmental Disorders. *Nature* **2017**, *542* (7642), 433−438.
(65) Larkin, M. A.; Blackshields, G.; Brown, N. P.; Chenna, R.; McGettigan, P. A.; McWilliam, H.; Valentin, F.; Wallace, I. M.; Wilm, A.; Lopez, R.; Thompson, J. D.; Gibson, T. J.; Higgins, D. G. Clustal W and Clustal X Version 2.0. *Bioinformatics* **2007**, *23* (21), 2947−2948.
(66) Waterhouse, A. M.; Procter, J. B.; Martin, D. M. A.; Clamp, M.; Barton, G. J. Jalview Version 2—a Multiple Sequence Alignment Editor and Analysis Workbench. *Bioinformatics* **2009**, *25* (9), 1189−1191.
(67) Heckman, K. L.; Pease, L. R. Gene Splicing and Mutagenesis by PCR-Driven Overlap Extension. *Nat. Protoc.* **2007**, *2* (4), 924−932.
(68) Chen, H.-K.; Fernandez-Funez, P.; Acevedo, S. F.; Lam, Y. C.; Kaytor, M. D.; Fernandez, M. H.; Aitken, A.; Skoulakis, E. M. C.; Orr, H. T.; Botas, J.; Zoghbi, H. Y. Interaction of Akt-Phosphorylated Ataxin-1 with 14−3-3 Mediates Neurodegeneration in Spinocerebellar Ataxia Type 1. *Cell* **2003**, *113* (4), 457−468.
(69) Dirk, B. S.; Pawlak, E. N.; Johnson, A. L.; Van Nynatten, L. R.; Jacob, R. A.; Heit, B.; Dikeakos, J. D. HIV-1 Nef Sequesters MHC-I Intracellularly by Targeting Early Stages of Endocytosis and Recycling. *Sci. Rep.* **2016**, *6* (1), 37021.
(70) Johnson, A. L.; Dirk, B. S.; Coutu, M.; Haeryfar, S. M. M.; Arts, E. J.; Finzi, A.; Dikeakos, J. D. A Highly Conserved Residue in HIV-1 Nef Alpha Helix 2 Modulates Protein Expression. *mSphere* **2016**, *1* (6), No. e00288-16.

https://doi.org/10.1021/acsomega.2c04014
ACS Omega 2022, 7, 34378−34388